High-resolution reservoir characterization using deep learning aided elastic full-waveform inversion: The North Sea field data example

*Zhen-dong Zhang** *and Tariq Alkhalifah**
**King Abdullah University of Science and Technology.*

SUMMARY

Reservoir characterization is an important component of oil and gas production, as well as prediction. Classic reservoir characterization algorithms, both deterministic and stochastic, are typically based on stacked images and rely on simplifications and approximations to the subsurface. Elastic full-waveform inversion, which aims to match the waveforms of pre-stack seismic data, can potentially provide more accurate high-resolution reservoir characterization from seismic data. However, full-waveform inversion can easily fail to characterize deep-buried reservoirs with strong anisotropic seals. We present a deep learning aided elastic full-waveform inversion strategy using observed seismic data and well logs available in the target area. Five facies are extracted from the well and then connected to the inverted P- and S-wave velocities using the trained neural networks, which corresponds to the distribution of facies in the subsurface. Such a distribution is further converted to the desired reservoir-related parameters such as velocities and anisotropy parameters using a proposed weighted summation. Finally, we further update these estimated parameters by matching the resulting simulated wavefields to the observed seismic data, which corresponds to another round of elastic full-waveform inversion. A North Sea field data example, the Volve Oil Field data set, is used to demonstrate our proposed method.

INTRODUCTION

The reservoir is defined as a subsurface body of rock having sufficient porosity and permeability to store and transmit fluids. It is a critical component of a complete petroleum system, and thus, its high-resolution characterization is one of the main objective of geophysical surveys. The majority of seismic methods currently used for reservoir characterization are interpretation based approaches (Partyka et al., 1999). Seismic attributes, which can be extracted from stacked images or pre-stack seismic data, are often converted to reservoir-related properties such as a fluid identifier or facies (Chopra and Marfurt, 2007). Extracting seismic attributes from migrated images can be stable in many cases but also requires true-amplitude imaging, which is also challenging in practice. The stochastic reservoir characterization, which aims to match the pre-stack seismic data, requires a reduction in the dimension of seismic attributes and also requires dense computational resources to converge (Eidsvik et al., 2004).

An alternative high-resolution reservoir characterization approach is to estimate the reservoir-related properties by matching the resulting simulated waveforms to the observed seismic ones. Elastic full-waveform inversion (FWI) has been used for fractured reservoir characterization in an ideal scenario, in which the background models were known (Zhang et al., 2017). The effective parameters such as the weaknesses or the orientations of fractures can be estimated by matching the waveforms of pre-stack seismic data. Such waveform inversion strategy faces two main problems in solving practical problems (Virieux and Operto, 2009): 1) simulated waveforms are often not close to the observed ones due to the incomplete physics used in the simulation and 2) crosstalk or leakage between the different parameters. Wave equations, either in an acoustic or even an elastic approximation, can mainly provide accurate traveltime/phase information, but often fail in representing the amplitudes. Seismic anisotropy, although it resides mostly in sediments, has a significant influence on seismic data (Tsvankin et al., 2010). The elimination of crosstalk between multiple parameters can be partially achieved by choosing an optimal parameterization. Meanwhile, a relatively large offset/depth ratio is needed to separate the contributions from different parameters (scattering angle dependent). Limited by the acquisition spread and the decay of signals at the far-offsets, not all the anisotropy parameters especially at the reservoir depth can be retrieved from surface collected seismic data. For example, ε acts as a garbage parameter in the parameterization of v_h, v_s, ε and η (Guitton and Alkhalifah, 2017). The interpretation of seismic data on its own will provide incomplete information due to the non-uniqueness and the limited spatial resolution. However, additional measurements that may illuminate the reservoir with varying coverage and resolution can provide considerable value (Hu et al., 2009).

Facies constrained elastic full-waveform inversion strategy can effectively reduce the crosstalk between different parameters by incorporating known facies (Zhang et al., 2018b). Facies, defined as groups of seismic properties and conformity layers that share a particular relationship with geological and lithological properties, can be obtained from wells, sedimentary histories or other investigations. Estimated models from seismic data and the extracted facies from other geophysical surveys, like well logs, are often at very different scales and there are no explicit formulas to merge such information. Previously, a Bayesian based inversion was used to connect such different information in a statistical matter (Zhang et al., 2018b). However, recently emerging machine learning can do a better job in finding statistical relationships between different types of data. In our proposed approach, we train deep neural networks (DNNs) to build the connection between the estimated models from seismic data and the known facies. In this way, a list of facies is mapped on to a 2D/3D inverted model, which is also known as the distribution of facies. The distribution of facies can be converted to desired parameters such as velocities and anisotropy parameters. We then use the converted model parameters as the input for another round of elastic FWI.

In this abstract, we first use a correlation based elastic FWI to obtain v_p and v_s. Then we calibrate the measured depth of one nearby well using the check shot information and extract a list of facies from the well. The anisotropy parameters, ε and η, are calculated using Backus averaging. Three vertical profiles of estimated v_p, v_s and the corresponding facies are selected as input data features and labels for the deep neural networks, respectively. The trained DNNs are used to estimate the distribution of facies. Finally, we convert the distribution of facies to the parameterization in terms of v_h, v_s, ε and η and conduct another round of elastic FWI. A hierarchical anisotropy inversion using the estimated v_p and v_s as input is added for comparison. A two-component ocean-bottom-cable (OBC) data from the North Sea is used to demonstrate the proposed method.

CORRELATION BASED ELASTIC FWI

To avoid the often unreliable amplitudes, we use the global correlation as our objective function (Choi and Alkhalifah, 2012), which is given by

$$J(\mathbf{m}) = -\sum_s \sum_r \widehat{\mathbf{u}} \cdot \widehat{\mathbf{d}}, \tag{1}$$

where $\widehat{\mathbf{u}} = \frac{\mathbf{u}}{||\mathbf{u}||}$ and $\widehat{\mathbf{d}} = \frac{\mathbf{d}}{||\mathbf{d}||}$ are normalized predicted and observed data, respectively. The indexes s and r correspond to the source and receiver locations, respectively.

The inverse problem is solved using the first-order elastic wave equation (Vigh et al., 2014), which is given by

$$\begin{pmatrix} \rho\mathbf{I}_3 & 0 \\ 0 & \mathbf{C}^{-1} \end{pmatrix} \frac{\partial \Psi(\mathbf{x},t)}{\partial t} - \begin{pmatrix} 0 & E^T \\ E & 0 \end{pmatrix} \Psi(\mathbf{x},t) - \mathbf{f}(x_s,t) = 0, \tag{2}$$

where $\Psi(\mathbf{x},t) = (v_1, v_2, v_3, \sigma_1, \sigma_2, \sigma_3, \sigma_4, \sigma_5, \sigma_6)^T$ is a vector containing three particle velocities and six stresses, $\mathbf{I}_3$ is a 3 by 3 identity matrix. $\mathbf{C}$ is the stiffness matrix, E denotes space differentiation, and $\mathbf{f}(x_s,t)$ is the source located at x_s.

To obtain the gradient function of the proposed objective function, we take its derivative with respect to the model parameters as follows (Zhang et al., 2018a)

$$\frac{\partial J}{\partial \mathbf{m}} = \sum_s \sum_r \frac{\partial \mathbf{u}}{\partial \mathbf{m}} \cdot \left(\frac{1}{||\mathbf{u}||} \left(\widehat{\mathbf{u}} \left(\widehat{\mathbf{u}} \cdot \widehat{\mathbf{d}} \right) - \widehat{\mathbf{d}} \right) \right), \tag{3}$$

For the parameterization of $C_{ij}s$, the Fréchet derivative, $\frac{\partial u(C_{ij},x,t)}{\partial C_{ij}}$, is given by Vigh et al. (2014):

$$\frac{\partial u(C_{ij},s,x,t)}{\partial C_{ij}} = \frac{\partial C}{\partial C_{ij}} \mathbf{C}^{-1} \left(\frac{\partial \sigma}{\partial t} - \mathbf{f} \right)_{i=1,\ldots 6;\, j=i,\ldots,6} \tag{4}$$

$$and \left(\frac{\partial C}{\partial C_{ij}} \right)_{pq} = \begin{cases} 1, p=i, q=j \\ 1, p=j, q=i \\ 0, otherwise \end{cases}, \tag{5}$$

where σ denotes the stress component of the forward-propagated wavefield. $\frac{\partial C}{\partial C_{ij}}$ is a six-by-six matrix with elements defined in equation 5. Here we use the parameterization of C_{ij}, but the gradients for other parameters such as v_p and v_s can be derived using the chain rule. The model is updated iteratively using the l-BFGS method (Liu and Nocedal, 1989), which is written as

$$\mathbf{m} = \mathbf{m}_0 - \alpha \mathbf{H}^{-1} \mathbf{g}, \tag{6}$$

where α is the step length calculated by the standard line-search method, and $\mathbf{H}$ is the approximated Hessian matrix.

EXTRACTING FACIES FROM THE WELL

Seismic facies can be obtained from different sources such as well log, core analysis and sedimentation history. Here, we extract a list of facies from the well log as shown in Figure 1. The reservoir is located at 2.75-3.12 km depth, with a seal rock above it. The well log covers the depth around the reservoir layer and it is from a tilted well. We calibrate the depth of the top and bottom of the dominant layers using the check shot (red line). Five facies are extracted from the reservoir area by manually grouping the velocities. More experienced interpreters can utilize more advanced classifications of facies. The interpreted facies are used as labels in the supervised learning. We then calculate the anisotropy parameters ε and η using Backus averaging (Berryman et al., 1999) as shown in Figure 2. The delineated facies have different combinations in terms of v_p, v_s, ε and η as listed in Table 1. The seal rock has a strong anisotropy while the reservoir layer is almost isotropic.

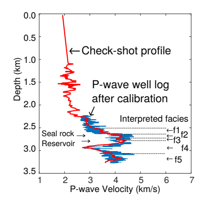

Figure 1: Depth-calibrated well log and extracted facies.

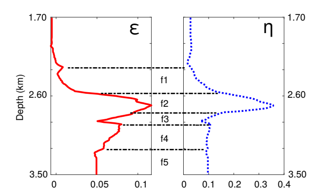

Figure 2: Calculated anisotropy parameters in terms of ε and η using Backus averaging.

Table 1: List of facies in the target area

	f1	f2	f3	f4	f5
v_p	3.45	4.2	4.0	3.1	4.1
v_s	1.7	2.4	2.2	1.5	2.4
ε	0.01	0.1	0.0	0.07	0.05
η	0.05	0.3	0.0	0.1	0.1

DEEP NEURAL NETWORKS

A deep neural network is nothing but a nonlinear system of equations that turns the input into the output (Van der Baan and Jutten, 2000). It has multiple hidden layers between the input and output layers. With the input layer denoted as $\mathbf{x}$, the kth hidden layer can be expressed as $\mathbf{a}_k = \sigma(\mathbf{W}_k\mathbf{x} + \mathbf{b}_k)$ and the output layer is written as $\mathbf{y} = \mathbf{W}\mathbf{a} + \mathbf{b}$. The input, $\mathbf{x}$, can be raw data or features (e.g., v_s/v_p) extracted from the data.

The output, $\mathbf{y}$, depends on the problem. For example, it can be 0 or 1 for labeling applications. The forward-propagation process utilizes the output of the previous layer as the input for the next layer. σ denotes the activation function, which defines the output of that node with fed input. It can be the sigmoid, rectified linear unit (ReLu) or some other functions. The training process updates $\mathbf{W}$ and $\mathbf{b}$ for each layer to seek a more accurate mathematical manipulation capable of mapping the input to the output using a loss function of sparse softmax cross entropy. We use three features, v_p, v_s and v_s/v_p, as inputs. Four hidden layers with 256 nodes in each layer are deployed as shown in Figure 3. A ReLu activation function is used. For each layer, we use a random dropout of 10% to avoid overfitting (Srivastava et al., 2014). Besides, A random data augmentation is applied to balance the proportion of different facies in training the data. The Adam gradient is used to update the weighting matrix of neural networks. In our application, we output the probabilities for all facies instead of one specific kind. After obtaining the percentages of being a certain facies, we can calculate the distribution of facies (converted to v_h, v_s, ε and η) by a weighted summation over n_f facies, $\bar{m} = \sum_{i=1}^{n_f} p_i m_i$. $\bar{m}$ denotes averaged P-, S-wave velocities or anisotropy parameters, which is equivalent to the posterior expectation in Zhang et al. (2018b). p_i and m_i are probabilities estimated by the trained DNNs and the known facies. Such a weighted summation avoids potential bias caused by a particular kind of facies when the DNNs fail. Besides, it can interpolate between different facies. In practice, we can never know all the facies in the subsurface and we do not need to know all of them in our proposed method. The probabilities act as interpolation weights for the known facies. If the corresponding facies for certain pairs of v_p and v_s is not available as prior knowledge, the averaged parameters still have a chance of being (or close to) the correct ones through interpolation.

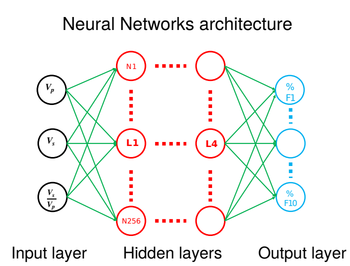

Figure 3: The Neural Network architecture. Three features are used in the input layer. Four hidden layers with 256 nodes are fully connected neural networks with a dropout rate of 10%. The output layer provides probabilities of being certain facies for the current input.

NUMERICAL EXAMPLES

We apply the proposed inversion strategy to a 2D line of the Volve data set. The seal layer and the reservoir, located at 2.75-3.12 km depth, are the main imaging goals. We use the raw data set with limited processing applied including polarity correction, instrumental deconvolution and data quality control. For the inversion, we use 240 shots and 240 two-component receivers distributed evenly at the distance of 50 m and 25 m, respectively. The length of the ocean-bottom cable (OBC) is 6 km and the sources are evenly distributed in 12 km just below the sea surface. A modified free-surface boundary condition, which can suppress strong surface waves, is used in the simulation (He et al., 2016). We convolve the observed data with the half-order differentiation of the known wavelet, and thus, we avoid source estimation, while correcting the phase discrepancy between the 3D acquisition and the 2D simulation (Pica et al., 1990; Yoon et al., 2012). The initial model is a 1D smoothed version of the model from the data owners shown in Figure 4. Only one frequency band (2-12 Hz) is used for the inversion. We first conduct the isotropic elastic FWI to estimate v_p and v_s as shown in Figure 5, then we apply a hierarchical vertical transverse isotropic (VTI) inversion (Oh and Alkhalifah, 2018), in which we use the parameterization v_h, v_s, ε and η as shown in Figure 6. The high-velocity seals and a relatively low-velocity layer appear in the inverted results. Finally, we train the deep neural networks to build the connection between the estimated v_p and v_s (Figure 5) and the extracted facies (Table 1). After training, we use all the model pixels to estimate the distribution of facies in the subsurface. The distribution of facies is further converted to v_h, v_s, ε and η using the proposed weighted summation. We use the converted v_h, v_s, ε and η as the initial model for another round of inversion and obtain the updated model as shown in Figure 7. The high-velocity seal rock with a strong anisotropy above a low-velocity zone is improved. Also, our proposed inversion managed to obtain a high-resolution ε and a lower-resolution η at the reservoir depth, which was guided by the data. Usually, η in the deeply buried seal rocks is not recoverable from the seismic data with limited offsets since it requires a relatively large offset/depth ratio (Alkhalifah and Plessix, 2014). The interleaved data comparison as shown in Figure 8 indicates that adding anisotropy effects can help us obtain simulated data that match the observed data better (Figures 8b and 8c). The deep learning aided approach can help improve the data matching in the far-offsets (Figures 8c and 8d). We plot the data-matching history for the different inversion scenarios as shown in Figure 9a. It shows that the isotropic inversion reduces the data misfit by 36% and the follow-up deep learning aided inversion can further reduce the data misfit by about an additional 10%. We also compare the inverted vertical P-wave velocities with the one from the check shot nearby in Figure 9b. The estimated vertical P-wave velocity using the proposed approach is close to the one from the check shot in the target depth. Remarkably, we did not use well logs or check shots as direct model constraints in the proposed inversion.

CONCLUSIONS

We develop a framework to invert for a relatively high resolution anisotropic description of the reservoir by utilizing surface seismic and facies information from a well, and using deep neural network (DNN) to connect them statistically. We applied this DNN-assisted elastic full waveform inversion on

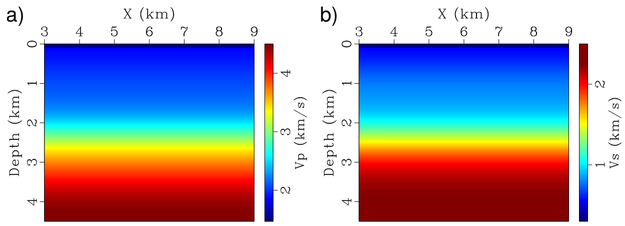

Figure 4: The initial models. a) v_p and b) v_s. They're 1D models.

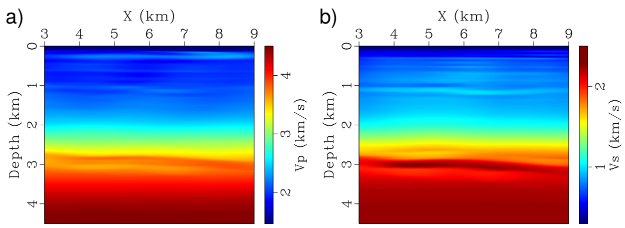

Figure 5: The inverted models using isotropy elastic FWI. a) v_p and b) v_s. The high-velocity seal rock is observable in v_p.

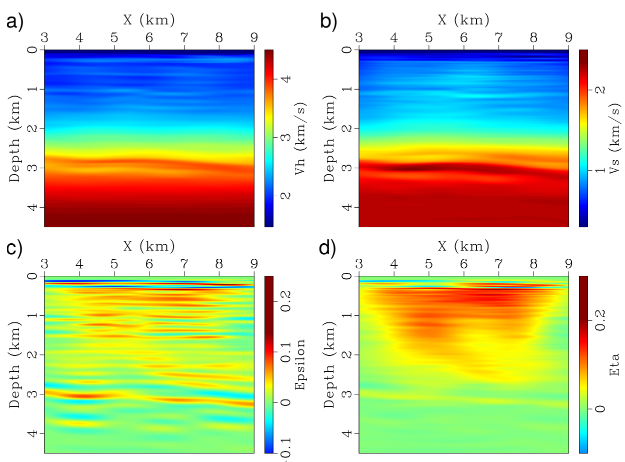

Figure 6: The inverted models using anisotropy elastic FWI. a) v_h, b) v_s, c) ε and d) η.

OBC data from the North sea, and obtained a reasonable inversion of the reservoir region.

ACKNOWLEDGMENTS

We want to thank Equinor and the former Volve license partners ExxonMobil E&P Norway AS and Bayerngas Norge AS, for the release of the Volve data. The views expressed in this paper are the views of the authors and do not necessarily reflect the views of Equinor and the former Volve field license partners. For computer time, this research used the resources of the Supercomputing Laboratory at King Abdullah University of Science & Technology (KAUST) in Thuwal, Saudi Arabia.

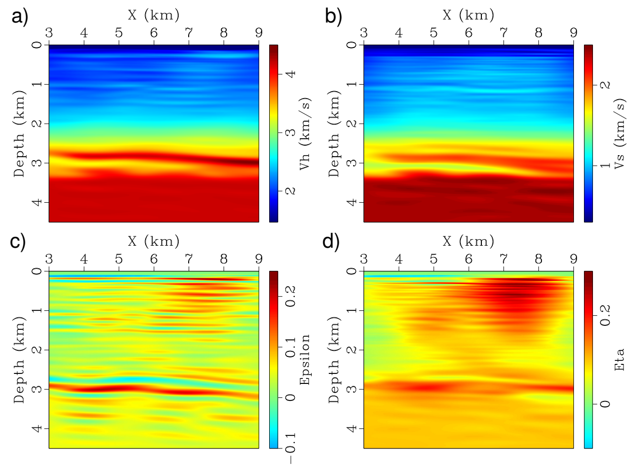

Figure 7: The inverted models using anisotropy elastic FWI with facies constraints. a) v_h, b) v_s, c) ε and d) η.

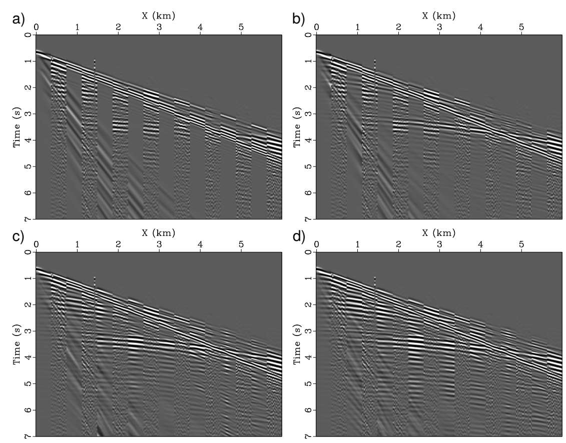

Figure 8: Shot gather displaying interleaved predicted and observed data using a) the initial v_p and v_s, b) the estimated v_p and v_s from isotropic inversion, c) the estimated v_h, v_s, ε and η from hierarchic VTI inversion and d) the deep learning aided VTI inversion.

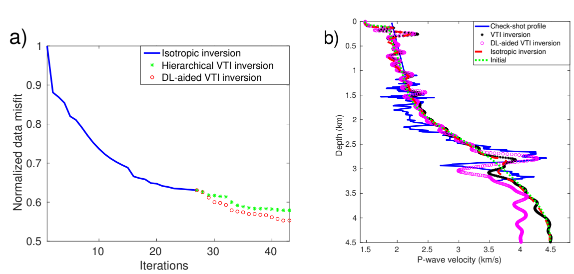

Figure 9: Data matching history a) and vertical P-wave velocity profiles b).

REFERENCES

Alkhalifah, T., and R.-É. Plessix, 2014, A recipe for practical full-waveform inversion in anisotropic media: An analytical parameter resolution study: Geophysics, **79**, R91–R101.

Berryman, J. G., V. Y. Grechka, and P. A. Berge, 1999, Analysis of Thomsen parameters for finely layered VTI media: Geophysical Prospecting, **47**, 959–978.

Choi, Y., and T. Alkhalifah, 2012, Application of multi-source waveform inversion to marine streamer data using the global correlation norm: Geophysical Prospecting, **60**, 748–758.

Chopra, S., and K. J. Marfurt, 2007, Seismic attributes for prospect identification and reservoir characterization: Society of Exploration Geophysicists and European Association of .

Eidsvik, J., P. Avseth, H. Omre, T. Mukerji, and G. Mavko, 2004, Stochastic reservoir characterization using prestack seismic data: Geophysics, **69**, 978–993.

Guitton, A., and T. Alkhalifah, 2017, A parameterization study for elastic vti full-waveform inversion of hydrophone components: Synthetic and North Sea field data examples: Geophysics, **82**, R299–R308.

He, W., R. Plessix, and S. Singh, 2016, Modified boundary conditions for elastic inversion of active land seismic data in VTI media: Presented at the 78th EAGE Conference and Exhibition 2016.

Hu, W., A. Abubakar, and T. M. Habashy, 2009, Joint electromagnetic and seismic inversion using structural constraints: Geophysics, **74**, R99–R109.

Liu, D. C., and J. Nocedal, 1989, On the limited memory BFGS method for large scale optimization: Mathematical programming, **45**, 503–528.

Oh, J.-W., and T. Alkhalifah, 2018, Optimal full-waveform inversion strategy for marine data in azimuthally rotated elastic orthorhombic media: Geophysics, **83**, R307–R320.

Partyka, G., J. Gridley, and J. Lopez, 1999, Interpretational applications of spectral decomposition in reservoir characterization: The Leading Edge, **18**, 353–360.

Pica, A., J. Diet, and A. Tarantola, 1990, Nonlinear inversion of seismic reflection data in a laterally invariant medium: Geophysics, **55**, 284–292.

Srivastava, N., G. Hinton, A. Krizhevsky, I. Sutskever, and R. Salakhutdinov, 2014, Dropout: a simple way to prevent neural networks from overfitting: The Journal of Machine Learning Research, **15**, 1929–1958.

Tsvankin, I., J. Gaiser, V. Grechka, M. Van Der Baan, and L. Thomsen, 2010, Seismic anisotropy in exploration and reservoir characterization: An overview: Geophysics, **75**, 75A15–75A29.

Van der Baan, M., and C. Jutten, 2000, Neural networks in geophysical applications: Geophysics, **65**, 1032–1047.

Vigh, D., K. Jiao, D. Watts, and D. Sun, 2014, Elastic full-waveform inversion application using multicomponent measurements of seismic data collection: Geophysics.

Virieux, J., and S. Operto, 2009, An overview of full-waveform inversion in exploration geophysics: Geophysics, **74**, WCC1–WCC26.

Yoon, K., S. Suh, J. Cai, and B. Wang, 2012, Improvements in time domain FWI and its applications, *in* SEG Technical Program Expanded Abstracts 2012: Society of Exploration Geophysicists, 1–5.

Zhang, Z., T. Alkhalifah, J.-W. Oh, and I. Tsvankin, 2017, Estimation of fracture parameters using elastic full-waveform inversion, *in* SEG Technical Program Expanded Abstracts 2017: Society of Exploration Geophysicists, 3272–3276.

Zhang, Z., T. Alkhalifah, Z. Wu, Y. Liu, B. He, and J. Oh, 2018a, Normalized nonzero-lag crosscorrelation elastic full-waveform inversion: Geophysics, **84**, R15–R24.

Zhang, Z.-d., T. Alkhalifah, E. Z. Naeini, and B. Sun, 2018b, Multiparameter elastic full waveform inversion with facies-based constraints: Geophysical Journal International, **213**, 2112–2127.